nature catalysis

Article

https://doi.org/10.1038/s41929-026-01488-w

Mixed-valence $Co^{0/II}O_x$ clusters on silicalite-1 facilitate propane dehydrogenation to propene

Received: 18 September 2024

Accepted: 14 January 2026

Published online: 23 February 2026

Check for updates

Qiyang Zhang[1,2,6], Yuming Li[1,6], Xinxin Tian[2,3,6], Vita A. Kondratenko[2], Elizaveta A. Fedorova[2], Tong Yang[1], Xiangnong Ding[2], Dmitry E. Doronkin[4], Dan Zhao[2,4,5], Chun Deng[1], Huihui Chen[5], Shutao Xu[5], Anna Zanina[2], Stephan Bartling[2], Tatiana Otroshchenko[2], Yajun Wang[1], Zhen Zhao[1], Chunming Xu[1], Guiyuan Jiang[1] ✉, Haijun Jiao[2] ✉ & Evgenii V. Kondratenko[2] ✉

Understanding the nature of active sites in heterogeneous catalysts and how to create them purposefully opens up the possibility of tailored catalyst design. Here we report mixed-valence subnanometre CoO_x clusters, consisting of a few metallic Co^0 atoms on top of Co^{2+}, bound to a silicalite-1 support through lattice oxygen atoms as active species for non-oxidative propane dehydrogenation (PDH) to propene. Compared with commercial-like $PtSn/Al_2O_3$ and $K\text{-}CrO_x/Al_2O_3$ catalysts also tested in the present study, as well as other state-of-the-art Pt- or Co-containing PDH catalysts, this system showed high on-stream stability, propene productivity and selectivity at close-to-equilibrium propane conversion. Moreover, it showed durability in a series of PDH/regeneration cycles between 500 and 550 °C. The performance of this catalyst system is industrially attractive in terms of propene production costs, as suggested by our initial techno-economic assessment.

Propene is the second most important olefin after ethylene and is used in the chemical industry to produce polypropylene, solvents, acrylic acid and so on[1]. It is mainly produced as a by-product in energy-intensive processes involving the cracking of various crude oil fractions[2,3]. With limited oil reserves but an increasing production of shale gas containing propane, propane dehydrogenation (PDH) has become the basis for several technologies, accounting for around 11% of the propene produced[4]. These technologies use Pt-containing (Oleflex and STAR technologies) or Cr-containing (CATOFIN technology) catalysts that suffer from high costs or low selectivity for propene[1,5]. There are also environmental concerns due to the toxicity of Cr(VI) compounds and the need to use Cl_2 or Cl-containing compounds to regenerate the Pt-containing catalysts.

To overcome these shortcomings, catalysts based on oxides of Zn (refs. 6–8), Co (refs. 9–11), Fe (refs. 12,13), Ga (ref. 14), V (refs. 15,16) or Zr (refs. 17,18) have been developed, but these have not yet found large-scale implementation due to low productivity and selectivity under industrially relevant conditions. Although Co-containing catalysts are among the most studied alternatives, the desired improvement in their performance is hindered by uncertainties in the nature of their active sites. It is in general agreed that supported $Co^{II/II}O_x$ species, ranging from isolated species to nanoparticles, on the surface of fresh

[1]State Key Laboratory of Heavy Oil Processing, China University of Petroleum, Beijing, China. [2]Leibniz-Institut für Katalyse, Rostock, Germany. [3]Institute of Molecular Science, Shanxi University, Taiyuan, China. [4]Institute for Chemical Technology and Polymer Chemistry and Institute of Catalysis Research and Technology, Karlsruhe Institute of Technology, Karlsruhe, Germany. [5]National Engineering Research Center of Lower-Carbon Catalysis Technology, Dalian Institute of Chemical Physics, Chinese Academy of Sciences, Dalian, China. [6]These authors contributed equally: Qiyang Zhang, Yuming Li, Xinxin Tian. ✉e-mail: jianggy@cup.edu.cn; haijun.jiao@catalysis.de; Evgenii.kondratenko@catalysis.de

catalysts can undergo reduction under PDH conditions to yield either $Co^{II}O_x$ or metallic Co^0 species[19–21]. Importantly, such species can coexist, but as separated species. Against this background, most researchers assume that $Co^{II}O_x$ sites are responsible for the dehydrogenation of propane to propene, while metallic Co^0 species are involved in side reactions leading to C_1-C_2 hydrocarbons and coke[9,11,22–26]. Other researchers, including ourselves, suggest that metallic Co^0 species dehydrogenate propane to propene[19,20,27,28].

Here we present the fundamentals necessary to develop zeolitic catalysts based on cobalt that demonstrate high propene productivity and selectivity, as well as stability, making the catalysts attractive for industrial applications. The use of supports bearing silanols in combination with a strong electrostatic adsorption method to deposit CoO_x is key to the preparation of such catalysts. Through the combination of precise material synthesis, catalytic testing and complementary characterization, including density functional theory (DFT) calculations, we identified partially reduced subnanometre CoO_x clusters on the surface of silicalite-1 (S-1), a SiO_2-based support, as the active species. These clusters contain metallic Co^0 atoms that sit on top of oxidic Co^{2+} species, which are connected to the support through Co–O–Si bonds and formed from their oxidized $Co^{II}O_x$ counterparts under PDH conditions. The role of Co^0 in the active species is to reduce the barriers for the cleavage of C–H bonds in propane and to induce the formation of H_2 from surface H species, with the latter process being the rate-limiting step of PDH, thus ensuring high catalyst activity and propene selectivity in the PDH reaction. For example, the best-performing catalyst showed a selectivity for propene of >95% at 87% equilibrium propane conversion at 525 °C and 20 kPa propane.

Results

Catalysts and their PDH activity

To control CoO_x speciation, we prepared a series of Co-containing catalysts using different preparation methods and SiO_2-based supports, such as S-1, amorphous SiO_2, hexagonal mesoporous silica (HMS) or MCM-41. The motivation was to understand whether and how the specific surface area (SSA) of these supports with different morphologies (Supplementary Table 1 and Supplementary Fig. 1) and the type of OH group determine the nature of the CoO_x species and their performance in PDH. The 1.1Co-S-1 catalyst (in the catalyst abbreviations, the initial number represents the weight percentage of cobalt) exhibited a substantially higher propene formation rate than catalysts based on the other supports, despite all the materials being prepared using the same strong electrostatic adsorption (SEA) method with an identical cobalt content of 1.1 wt% (Fig. 1a and Supplementary Table 2). No correlation could be found between the formation rate and SSA or the volume ratio of micropores to mesopores (Supplementary Fig. 2), suggesting that other support properties are responsible for the formation of active CoO_x species.

The support effect evidenced in Fig. 1a can be related to the presence of defective OH groups (silanols) in the S-1 support (Fig. 1e). To understand the role of these defects, we synthesized a silicalite-1 support with a lower concentration of silanols (S-1_L) than in S-1 and used it to prepare a Co-containing catalyst (1.1Co-S-1_L) by the SEA method. All materials were characterized by solid-state ^{1}H NMR spectroscopy. The concentration of silanols decreased upon the introduction of cobalt (Fig. 1f, Supplementary Fig. 3 and Supplementary Table 3). Importantly, 1.1Co-S-1 showed higher PDH activity than 1.1Co-S-1_L (Fig. 1b), supporting the importance of the silanols. Moreover, the use of S-1 treated with $(NH_4)_2SiF_6$ (S-1_F) to heal the OH defects (Fig. 1g) resulted in a less active PDH catalyst (1.1Co-S-1_F), also prepared by the SEA method (Fig. 1c). This treatment was not found to change the SSA or pore volume of the support (Supplementary Fig. 2 and Supplementary Table 1). The decisive role of the silanols was further confirmed by the poor activity of 1.1Co-Na-S-1, prepared using a Na-S-1 support with 1.2 wt% Na content (Supplementary Fig. 4) in which the defects were occupied by Na^+ (Supplementary Fig. 5) without affecting the structure of the micropore support (Supplementary Fig. 2 and Supplementary Table 1). Finally, we de-aluminated β-zeolites with different Si/Al ratios (25 and 150) to create supports with different densities of silanol defects; the lower the Si/Al ratio, the higher the density of defects (Fig. 1h). A higher PDH activity was determined for 1.1Co-Deal Beta-25 than for 1.1Co-Deal Beta-150, with both materials prepared by the SEA method (Fig. 1d). However, the presence of silanols is not the only factor affecting catalyst activity. The 1.1Co-S-1 catalyst showed a substantially higher rate of propene formation than its counterparts prepared by traditional impregnation (1.1Co/S-1_IM), hydrothermal (1.1Co@S-1_HY) and solid-phase grinding (1.1Co/S-1_SPG) methods (Supplementary Fig. 6). Thus, the method of preparation and the presence of silanols are both key factors in the formation of CoO_x species with a specific structure as discussed below.

Industrial relevance and benchmarking

Inspired by the high intrinsic activity of 1.1Co-S-1, we performed PDH tests with a propane conversion of at least 60% of the equilibrium conversion at various reaction temperatures using a feed with 40 vol% C_3H_8 to check the industrial potential of the catalyst. The obtained space–time yield of propene formation ($STY(C_3H_6)$) and propene selectivity ($S(C_3H_6)$) are presented in Fig. 2a,b, together with the corresponding data previously reported for state-of-the-art Co-containing catalysts (Supplementary Table 4). As PDH is a reversible reaction, the equilibrium propane conversion ($X(C_3H_8)_{eq}$) is influenced by the propane feed concentration, reaction temperature and total pressure. The lower the concentration and pressure and the higher the temperature, the higher the propane conversion. Thus, to ensure a proper comparison of the catalysts tested under different reaction conditions, we used the ratio of the experimentally determined propane conversion to the equilibrium conversion ($X(C_3H_8)_{exp}/X(C_3H_8)_{eq}$). In general, for any PDH catalyst, the closer this ratio is to 1, the lower the $STY(C_3H_6)$ and $S(C_3H_6)$ values will be due to the approach to equilibrium and subsequent propene transformations, respectively. The $STY(C_3H_6)$ values achieved at 500, 550 and 600 °C were 1.4, 3.0 and 4.2 kg C_3H_6 per kg catalyst per h at a propane conversion of about 65%, 77% and 82% of the equilibrium conversion, respectively (Supplementary Figs. 7 and 8). As propene is the main precursor of carbon deposits, the propene selectivity of about 90% obtained over 1.1Co-S-1 at an outlet propene concentration ($C(C_3H_6)_{out}$) of about 18 vol% and a propane conversion of 82% of the equilibrium conversion is remarkable and has not been reported before (Fig. 2b and Supplementary Table 4).

The 1.1Co-S-1 catalyst was also directly compared with the commercial analogues $PtSn/Al_2O_3$ and $K\text{-}CrO_x/Al_2O_3$ tested in parallel at 500 °C using a feed with 40 vol% C_3H_8 (Fig. 2c and Supplementary Fig. 9). The developed catalyst and $PtSn/Al_2O_3$ reached about 67% equilibrium propane conversion, which was about 2.5 times higher than that of $K\text{-}CrO_x/Al_2O_3$. This is noteworthy because Pt-based catalysts are typically more active than those based on non-noble metal oxides[1]. The conversion over 1.1Co-S-1 barely changed during a time on stream of 12 h, but decreased over $PtSn/Al_2O_3$ and $K\text{-}CrO_x/Al_2O_3$. For all catalysts, the selectivity for propene was above 97% and did not change with increasing time on stream. Compared with previously tested Pt-based catalysts, the 1.1Co-S-1 catalyst also showed high propene selectivity at high outlet propene concentrations (Fig. 2d and Supplementary Table 5).

Using a feed with 95 vol% C_3H_8, the conversion of propane over 1.1Co-S-1 decreased only slightly during a time on stream of 96 h, while the selectivity for propene increased to about 98% (Supplementary Fig. 10). The apparent deactivation rate constant (k_d) calculated in this experiment was only $1.6 \times 10^{-3}\ h^{-1}$. This value is substantially lower than those reported for other metal oxide-based catalysts, which also showed less activity (Supplementary Fig. 11 and Supplementary Table 6). Using the approach of Motagamwala et al.[29], who introduced a highly efficient Pt-containing catalyst operating at thermodynamic equilibrium, we calculated the ratio of the initial

https://doi.org/10.1038/s41929-026-01488-w

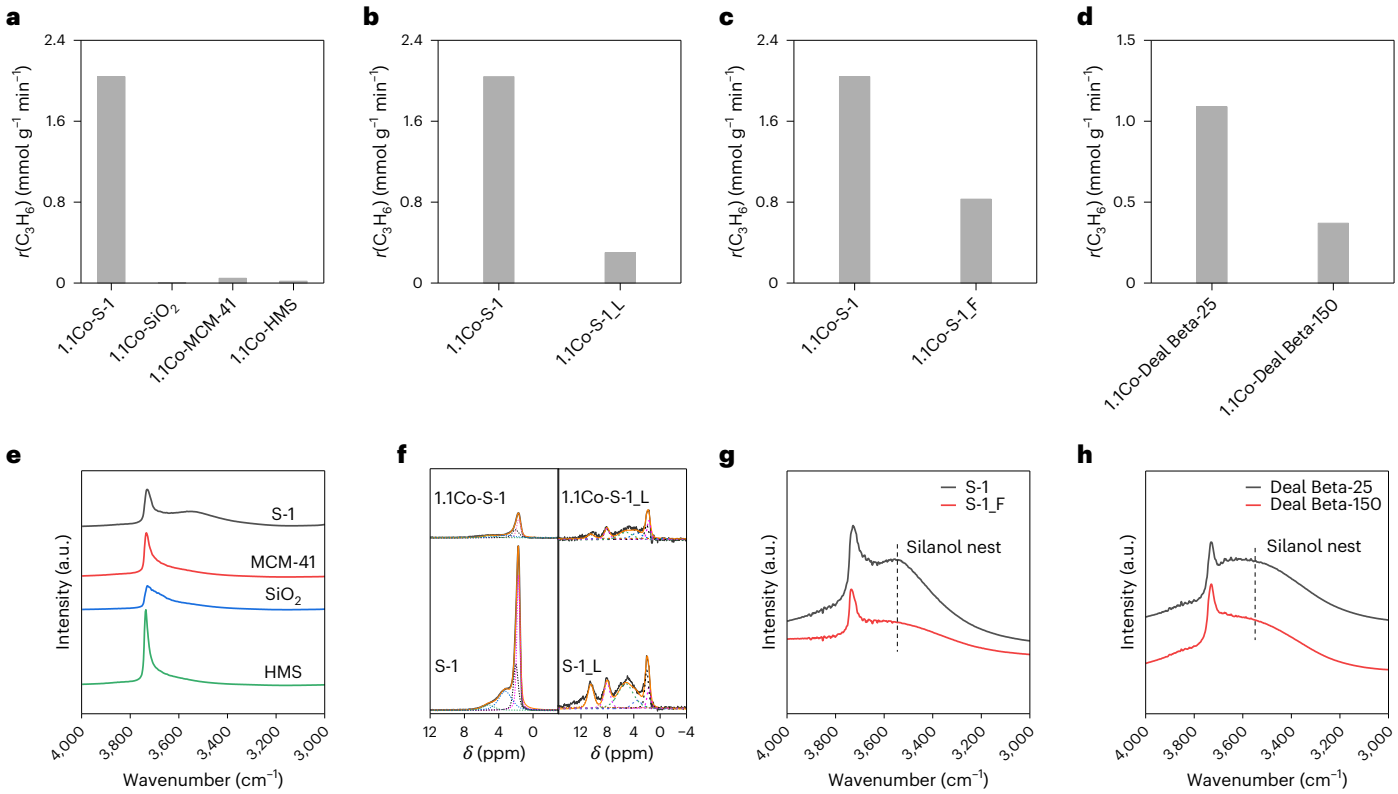

Fig. 1 | Catalyst activity and silanol characterization. a–**d**, Propene formation rate over 1.1Co-S-1, 1.1Co-SiO_2, 1.1Co-MCM-41 and 1.1Co-HMS (**a**), 1.1Co-S-1 and 1.1Co-S-1_L (**b**), 1.1Co-S-1 and 1.1Co-S-1_F (**c**), and 1.1Co-Deal Beta-25 and 1.1Co-Deal Beta-150 (**d**). Reaction conditions: T = 500 °C, weight hourly space velocity of C_3H_8 (WHSV(C_3H_8)) = 70.7 h^{-1} and C_3H_8/N_2 = 2:3. **e**, In situ Fourier transform infrared (FTIR) spectra of S-1, MCM-41, SiO_2 and HMS. **f**, Solid-state ^{1}H NMR spectra of the bare S-1 and S-1_L supports, as well as the 1.1-Co-S-1 and 1.1-Co-S-1_L catalysts. **g**, In situ FTIR spectra of S-1 and S-1_F. **h**, In situ FTIR spectra of Deal Beta-25 and Deal Beta-150. The spectra were recorded at 500 °C in a flow of N_2 (10 ml min^{-1}) after pre-treatment of the catalyst in air at 500 °C for 1 h.

forward rate of propene formation to k_d. Motagamwala et al. referred to this ratio as the overall catalyst productivity. A comparison of this ratio for our 1.1Co-S-1 catalyst with the data derived by Motagamwala et al. for various PDH catalysts reported in the literature showed that the performance of 1.1Co-S-1 is noteworthy (Fig. 3a and Supplementary Table 7), further demonstrating its application potential. The ability of catalysts to recover their initial performance after oxidative regeneration is another key property relevant to commercial applications. The 1.1Co-S-1 catalyst showed durable operation over 120 PDH/regeneration cycles at 500 and 525 °C, and over 20 PDH/regeneration cycles at 500 and 550 °C (Fig. 3b,c and Supplementary Figs. 12 and 13) using a feed with 20 or 40 vol% propane. The size of the CoO_x species was observed to change only slightly after 120 PDH/regeneration cycles[30] (Supplementary Fig. 14).

According to our techno-economic assessment using the Aspen software, the costs of propene production when operating even at 525 °C with a total pressure of 0.20 bar using pure C_3H_8 would be comparable to the CATOFIN technology if the selectivity for propene were above 95% at a propane conversion of at least 87% of the equilibrium conversion (Supplementary Figs. 15–17 and Supplementary Tables 8–11). Operation at such a low temperature would be advantageous for high propene selectivity as cracking reactions would be hindered.

Catalytically active species and their structure

To identify the structure of the supported CoO_x species showing high PDH activity, the prepared catalysts were thoroughly characterized using state-of-the-art complementary methods. X-ray diffraction (XRD) analysis of all of the prepared catalysts revealed only reflections characteristic of the support (Supplementary Fig. 18). No crystalline CoO or Co_3O_4 was identified in the catalysts by XRD. However, X-ray amorphous Co_3O_4 particles were detected in the 1.1Co/S-1_IM, 1.1Co-Na-S-1 and 2.9Co-S-1 catalysts by UV–visible spectroscopy (Supplementary Fig. 19). These particles were absent in the other catalysts, as confirmed by UV–visible spectroscopy (Supplementary Fig. 19) and high-resolution transmission electron microscopy (TEM; Supplementary Figs. 20–27). Ultrasmall CoO_x clusters on the surface of 1.1Co-S-1 were identified by aberration-corrected high-angle angular dark-field scanning TEM (AC-HAADF-STEM; Fig. 4a,b), with an average size of about 0.74 nm.

The local structure of the supported CoO_x species was elucidated by X-ray absorption spectroscopy (XAS). The Fourier transform (FT) k^2-extended X-ray absorption fine structure (EXAFS) spectra are shown in Fig. 4c and Supplementary Fig. 28. According to the EXAFS fits (Supplementary Figs. 29 and 30 and Supplementary Table 12), low-intensity Co–O–Co and Co–O–Si features are present in the spectrum of 1.1Co-S-1, suggesting the presence of small CoO_x clusters, while the 1.1Co/S-1_IM and 1.1Co-Na-S-1 samples contain large Co_3O_4 particles. As only features of Co–O–Si could be identified in the spectra of the other catalysts, they should contain isolated CoO_x species. For all of the catalysts, the oxidation state of cobalt was determined to be 2+, as deduced from the pre-edge peak at 7,709.5 eV in the X-ray absorption near-edge structure (XANES) spectra (Supplementary Fig. 28)[24].

We also investigated whether and how the structure of the CoO_x clusters and the oxidation state of the metal change when the 1.1Co-S-1 catalyst is exposed to H_2 and C_3H_8. The catalyst was first heated to 500 °C in He, then subjected to a flow of 50 vol% H_2 in He for 30 min, followed by a flow of 50 vol% C_3H_8 in He for 30 min (Fig. 4d). The treatment with H_2 resulted in the formation of metallic Co–Co bond(s), as concluded from the EXAFS fit (Supplementary Fig. 31 and Supplementary Table 13). Based on linear combination analysis (Supplementary Fig. 32) of the XANES spectra recorded at the Co K edge, the catalyst contains about

https://doi.org/10.1038/s41929-026-01488-w

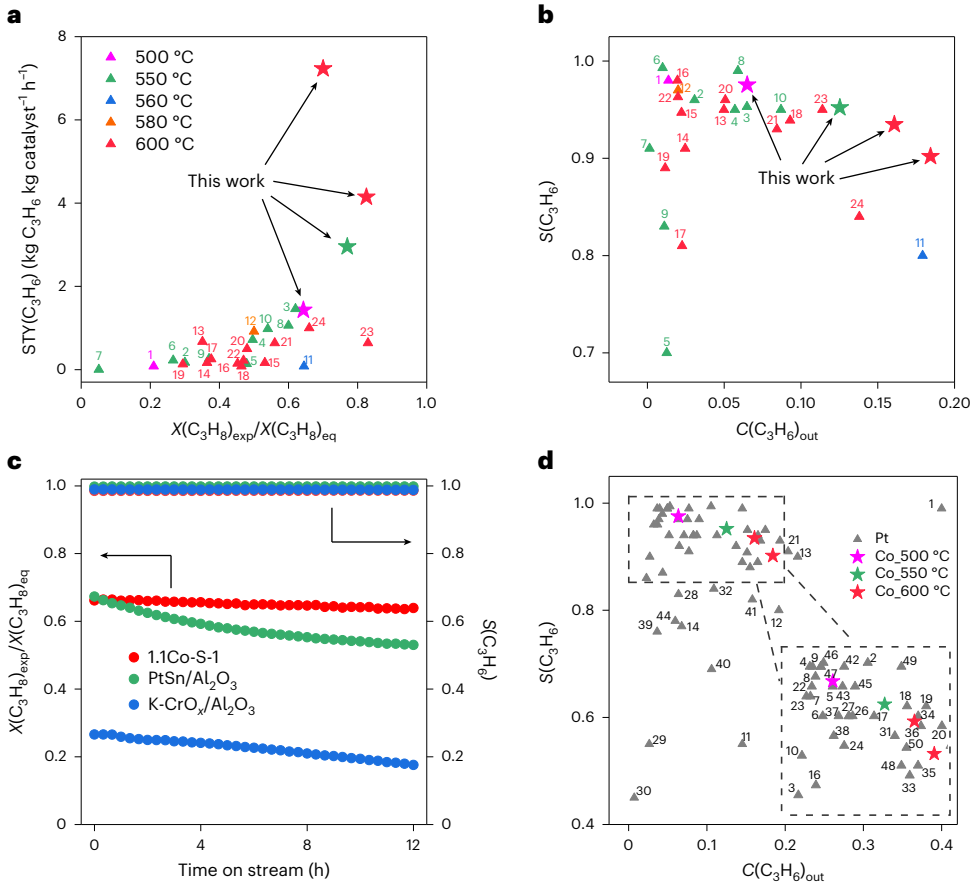

Fig. 2 | Comparison of 1.1Co-S-1 performance with state-of-the-art catalysts. **a**, $STY(C_3H_6)$ over 1.1Co-S-1 and previously tested catalysts at different temperatures versus $X(C_3H_8)_{exp}/X(C_3H_8)_{eq}$. **b**, $S(C_3H_6)$ versus $C(C_3H_6)_{out}$ determined in PDH over 1.1Co-S-1 and other Co-based catalysts. **c**, Time-on-stream profiles of $X(C_3H_8)_{exp}/X(C_3H_8)_{eq}$ and $S(C_3H_6)$ over 1.1Co-S-1 and the commercial analogues $PtSn/Al_2O_3$ and $K\text{-}CrO_x/Al_2O_3$. **d**, $S(C_3H_6)$ versus $C(C_3H_6)_{out}$ determined in PDH over 1.1Co-S-1 and various Pt-based catalysts. The dashed box in the bottom right-hand corner provides an enlarged view of the region highlighted by the dashed box in the top left-hand corner. Co_500 °C, Co_550 °C and Co_600 °C denote the $S(C_3H_6)$ values obtained over 1.1Co-S-1 at 500 °C, 550 °C and 600 °C, respectively. Reaction conditions for **a**, **b** and **d**: T = 500–600 °C, C_3H_8/N_2 = 2:3, and $WHSV(C_3H_8)$ = 9.4 and 18.8 h^{-1}; reaction conditions for **c**: T = 500 °C, C_3H_8/N_2 = 2:3 and $WHSV(C_3H_8)$ = 5.4 h^{-1}. The numbers in **a** and **b** correspond to the row numbers in Supplementary Table 4; the numbers in **d** correspond to the row numbers in Supplementary Table 5.

19% metallic Co^0 after 30 min under a stream of H_2. No further formation of metallic Co^0 was observed when the catalyst was further treated with C_3H_8 for 30 min at the same temperature (Fig. 4d).

We used in situ UV–visible spectroscopy in combination with chemical titration of metallic Co^0 with O_2 to independently validate the reducibility of CoO_x. The 1.1Co-S-1 catalyst was first treated with a flow of H_2 (H_2/Ar = 2:3) at 500 °C for 30 min. H_2, and not C_3H_8, was used in these tests to circumvent the formation of coke. The reduction of CoO_x is a fast process, as concluded from the temporal changes in the UV–visible spectra under the flow of H_2 (Fig. 4e). The intensity of the broad band at 330 nm, assigned to charge-transfer transitions between O^{2-} and Co^{2+} (ref. 30), decreased strongly within the first 2 min under a stream of H_2. No further changes were observed with increasing treatment time. The bands at 504, 594 and 672 nm are associated with the splitting of the $4A_2 \rightarrow {}^4T_1(P)$ band due to Jahn–Teller distortion of the tetrahedral Co^{2+} ions. The reduced catalyst was re-oxidized in a flow of O_2 (O_2/Ar = 1:4) at the same temperature. The amount of O_2 consumed was determined using an on-line mass spectrometer (Supplementary Fig. 33). The consumption was exclusively due to the re-oxidation of Co^0 formed during the preceding treatment with H_2. Using the amount of O_2 consumed, the fraction of Co^0 was calculated to be 22%.

Pseudo in situ X-ray photoelectron spectroscopy (XPS) measurements proved the presence of Co^0 in the 1.1Co-S-1 catalyst after treatment in a flow of 40 vol% H_2/N_2 at 500 °C for 30 min (Supplementary Fig. 34). Analysis showed that the fresh catalyst contains exclusively Co^{2+}, with its characteristic satellite features, while a distinct peak corresponding to Co^0 at 777.5 eV (ref. 20) was observed in the XPS spectrum of the reduced catalyst (Fig. 4f). Approximately 27% of Co^{2+} was reduced to Co^0, which is close to the values of 22% and 19% determined from the O_2 titration tests and in situ XAS characterization discussed above.

To understand how the degree of reduction of CoO_x species affects PDH activity, we first elucidated the reducibility of S-1-based catalysts with differing size of CoO_x species. To this end, additional catalysts were prepared by an impregnation method (Supplementary Fig. 35). Temperature-programmed reduction (TPR) tests with H_2 revealed significant differences in the reducibility of the catalysts (Supplementary Fig. 36). The average reduction degree (RD(TPR)) of CoO_x calculated from the amount of H_2 consumed between 100 and 600 °C and the actual concentration of cobalt increase with increasing size of the CoO_x species (Fig. 5a and Supplementary Table 14). The same correlation was obtained using the average reduction degree (RD(pulse)) of CoO_x calculated from the amount of O_2 consumed by the fresh catalysts reduced in a flow of H_2/Ar = 4:6 (20 ml min^{-1}) at 500 °C for 30 min (Supplementary Figs. 37 and 38). The reducibility–size effect was confirmed by DFT calculations (Supplementary Fig. 39 and Supplementary Table 15).

https://doi.org/10.1038/s41929-026-01488-w

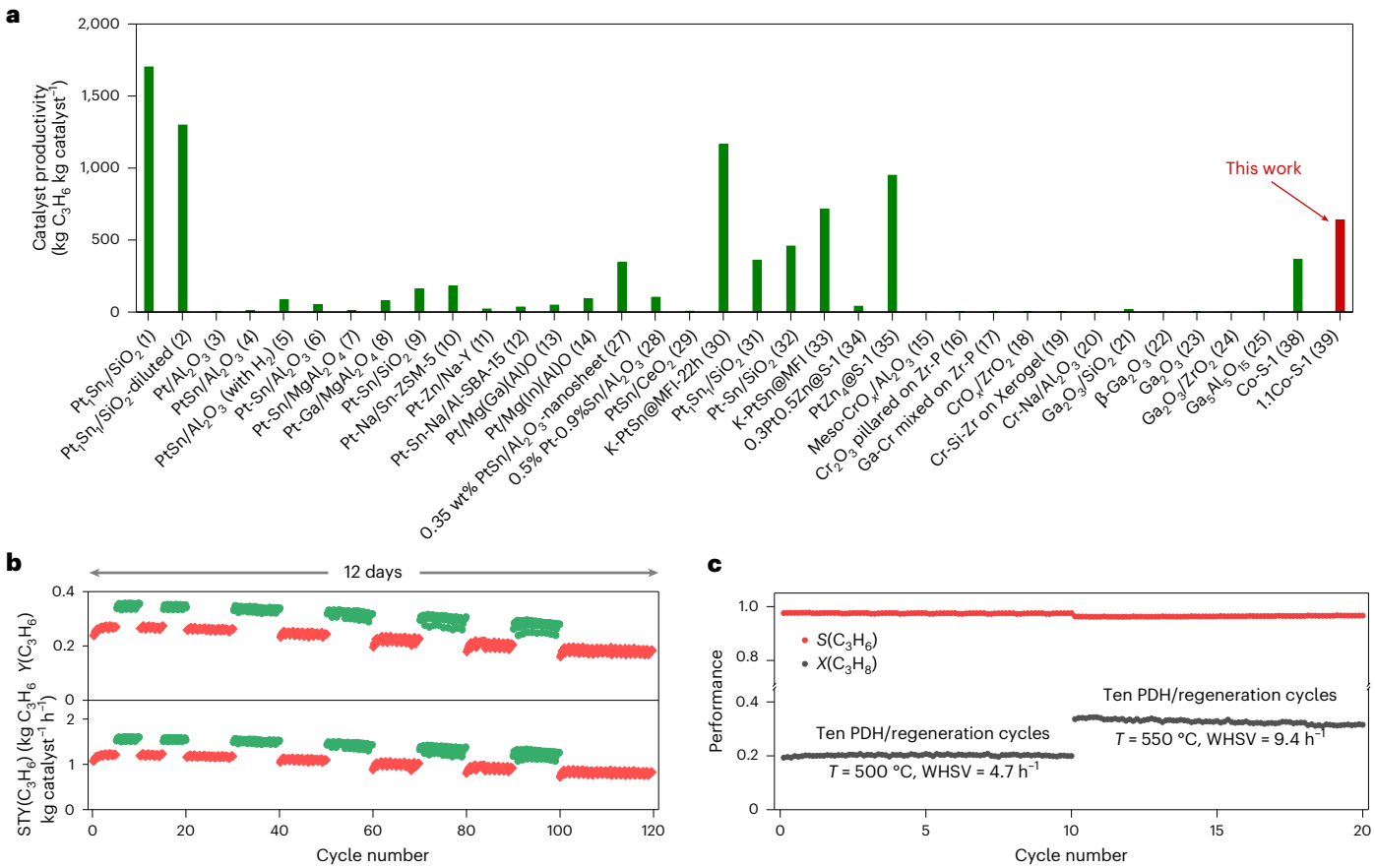

Fig. 3 | Productivity and durability of the 1.1Co-S-1 catalyst. a, Overall catalyst productivity of 1.1Co-S-1 and other PDH catalysts reported by Motagamwala et al.[29] (the numbers in parentheses correspond to the row numbers in Supplementary Table 7). **b**, On-stream profiles of yield of C_3H_6 ($Y(C_3H_6)$) and $STY(C_3H_6)$ over 1.1Co-S-1 in a series of 120 PDH/regeneration cycles performed at 500 °C (red) and 525 °C (green). Reaction conditions: T = 500–525 °C, C_3H_8/N_2 = 1:4 and $WHSV(C_3H_8)$ = 4.7 h^{-1}. **c**, On-stream profiles of $X(C_3H_8)$ and $S(C_3H_6)$ over 1.1Co-S-1 in a series of 20 PDH/regeneration cycles performed at 500 and 550 °C (10 cycles each). Reaction conditions: C_3H_8/N_2 = 2:3 and $WHSV(C_3H_8)$ = 4.7 and 9.4 h^{-1} at 500 and 550 °C, respectively.

Importantly, the initial rate of propene formation passes a maximum with increasing reduction degree of CoO_x (Fig. 5b). When the most-active 1.1Co-S-1 catalyst was reduced at 550 or 600 °C (1.1Co-S-1_R550 and 1.1Co-S-1_R600, respectively), the reduction degree increased from 21% to 31% or 40%, respectively (Supplementary Fig. 40). Compared with 1.1Co-S-1 reduced at 500 °C (1.1Co-S-1_R500), the rate of propene formation over the catalyst reduced at 550 °C increased slightly, but a decrease was observed for the catalyst reduced at 600 °C (Supplementary Fig. 41). These results fit with the observation in Fig. 5b, suggesting a synergistic effect between metallic Co^0 and Co^{2+} on catalyst activity. Moreover, an optimal ratio between these two oxidation states of cobalt seems to be required to achieve the highest effect.

As the experimental results discussed above do not resolve whether Co^0 and Co^{2+} in the 1.1Co-S-1 catalyst under PDH conditions are separated or coexist in a single species on the surface of the support, we performed DFT calculations to gain insights in this regard. We found that Co^0 atoms interact very weakly with non-defective support sites (−0.64 eV; Supplementary Fig. 42) and thus can easily diffuse into the S-1 channels. On this basis, we can expect the formation of large Co^0 nanoparticles. However, such species have not been identified experimentally by XAS. DFT calculations also predict that Co^0 atoms can be easily oxidized to Co^{2+} by surface hydroxy groups[31,32]. Therefore, we propose that partially reduced CoO_x species formed under PDH conditions should not comprise small Co^0 clusters separated from $Co^{II}O_x$, but Co^0 atoms connected to Co^{2+} sites. However, what would be the structure of the partially reduced CoO_x clusters?

Based on our XAS and AC-HAADF-STEM experimental data, as well as previous representative models of small CoO_x clusters[33], we constructed an embedded, oxidized Co_4O_6 cluster ($(Si{-}O)_4Co_4O_2$) at the hydroxy nest of the T5 S-1 site. This site is the tetrahedral (T) crystallographically distinct framework site in the MFI topology. It is located at the intersection of the straight and sinusoidal ten-membered ring channels. All four OH groups were consumed to initially yield Co_2O_4 ($4OH + 2Co(OH)_2 \rightarrow Co_2O_4 + 4H_2O$), followed by the addition of a Co_2O_2 unit ($Co_2O_4 + Co_2O_2$). In this structure, there are four Co–O–Si and two Co–O units ($(Si{-}O)_4Co_4O_2$). Thus, all Co atoms have the formal oxidation state of 2+. The cluster can exist as a nearly planar (0 eV) or Co_4O_6 cubic-like (1.47 eV) structure (Supplementary Fig. 43). As the former structure is more stable, it was used to create a partially reduced Co_4O_4 ($Co_2O_4 + 2Co$) cluster ($(Si{-}O)_4Co_4$) by removing two oxygen species bound to Co^{2+} (Supplementary Fig. 44). This cluster consists of two formal Co^0 centres on the top of two formal Co^{2+}.

Reactivity of oxidized and partially reduced CoO_x in PDH

If partially reduced supported CoO_x species were responsible for the high PDH activity, the rate of propene formation would decrease in the presence of co-fed oxygen. To verify this hypothesis, we performed catalytic tests using a reaction feed with 40 vol% C_3H_8 and 0.1 vol% O_2. A strong inhibitory oxygen effect was identified at both 500 °C (Fig. 6a) and 550 °C (Supplementary Fig. 45). The selectivity for propene was also negatively influenced.

Further insights into the role of oxidized or partially reduced CoO_x clusters in PDH were derived from temporal analysis of the products

https://doi.org/10.1038/s41929-026-01488-w

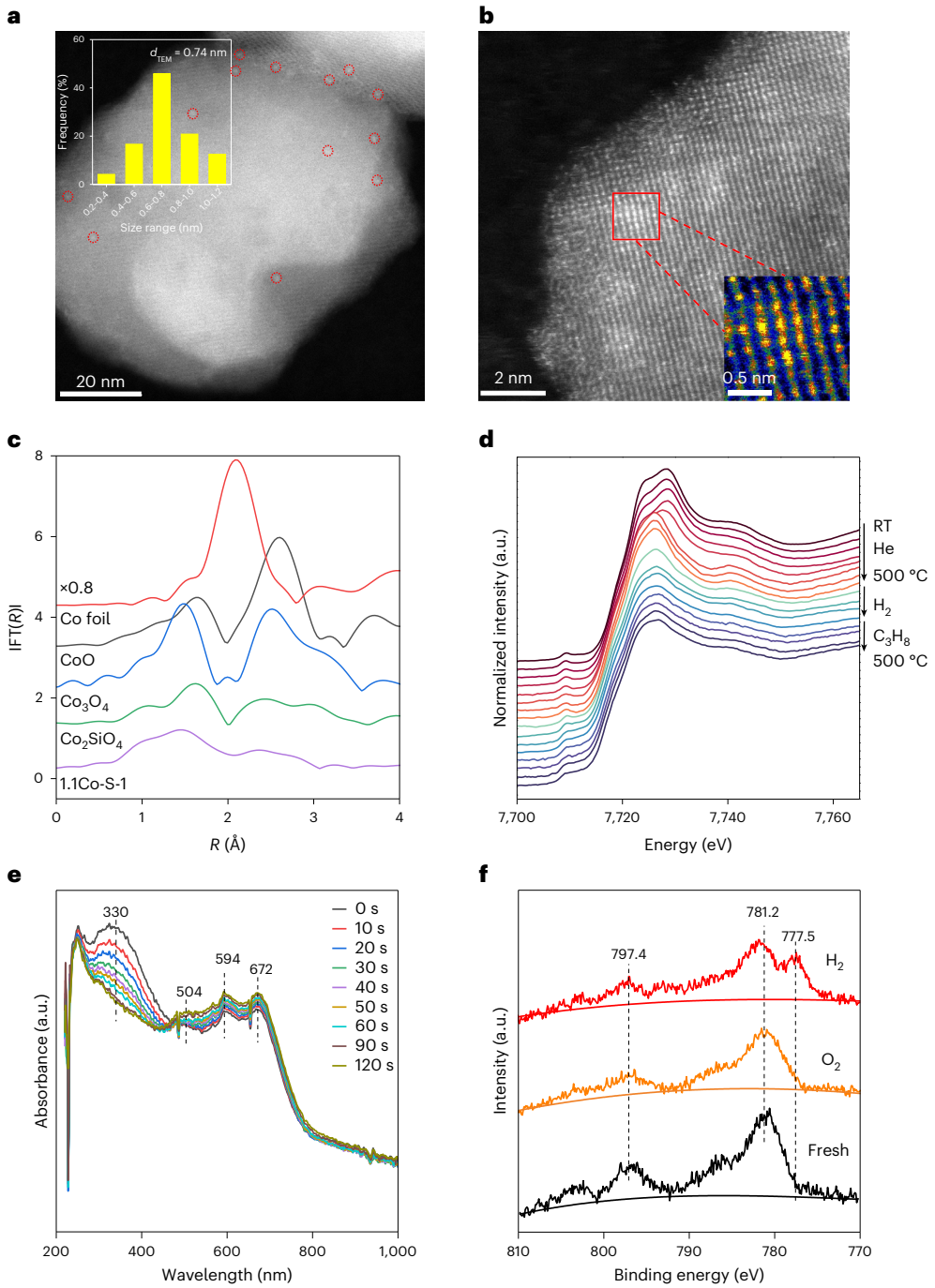

Fig. 4 | Characterization of 1.1Co-S-1. a,**b**, AC-HAADF-STEM images of 1.1Co-S-1 with the insets showing the size distribution of the CoO_x species (**a**) and an enlarged view of the region highlighted by the red square (**b**). d_{TEM} in the inset in **a** means the diameter of CoO_x determined by TEM. **c**, EXAFS spectra of 1.1Co-S-1 and reference samples CoO, Co_3O_4, Co_2SiO_4 and Co foil. The spectra are Fourier-transformed ('IFT(*R*)I') without phase correction. **d**, In situ XANES spectra at the Co K edge during heating from room temperature (RT) to 500 °C in He, followed by reduction in 50 vol% H_2/He and then switching to a flow of 50 vol% C_3H_8/He at 500 °C. **e**, In situ UV–visible spectra recorded in the first 2 min of treatment of 1.1Co-S-1 in 40 vol% H_2 at 500 °C. **f**, In situ XPS spectra of fresh 1.1Co-S-1 and the catalyst after treatment at 500 °C in 20 vol% O_2 and 40 vol% H_2.

(TAP) with submillisecond resolution. A series of approximately 3 nmol C_3H_8 pulses were introduced over 1.1Co-S-1 either oxidized in 50 vol% O_2 in N_2 or reduced in 20 vol% H_2 in N_2 at 500 °C. In addition to C_3H_6, CO_2 and H_2O were also formed when the oxidized catalyst was treated with C_3H_8 (Fig. 6b). As no gas-phase O_2 was co-pulsed with C_3H_8, the lattice oxygen of oxidized CoO_x must be involved in the formation of these products. The concentration of CO_2 decreased with increasing number of C_3H_8 pulses due to the irreversible consumption of lattice oxygen in the CoO_x species, resulting in their partial reduction (Supplementary Fig. 46). Finally, C_3H_6 and H_2 became the only products. These products were exclusively formed when C_3H_8 was pulsed over the reduced catalyst already containing Co^0 (Fig. 6c). Thus, the PDH reaction takes place over partially reduced CoO_x. Although the maximum concentrations of H_2 and C_3H_6 are achieved at very similar times, their rates of formation must be different, with the formation of H_2 being slower for the following reasons. As the diffusion coefficient of H_2 is about 4.6 times higher than that of C_3H_6, this product appears earlier at the reactor outlet. Therefore, we converted the experimental time

https://doi.org/10.1038/s41929-026-01488-w

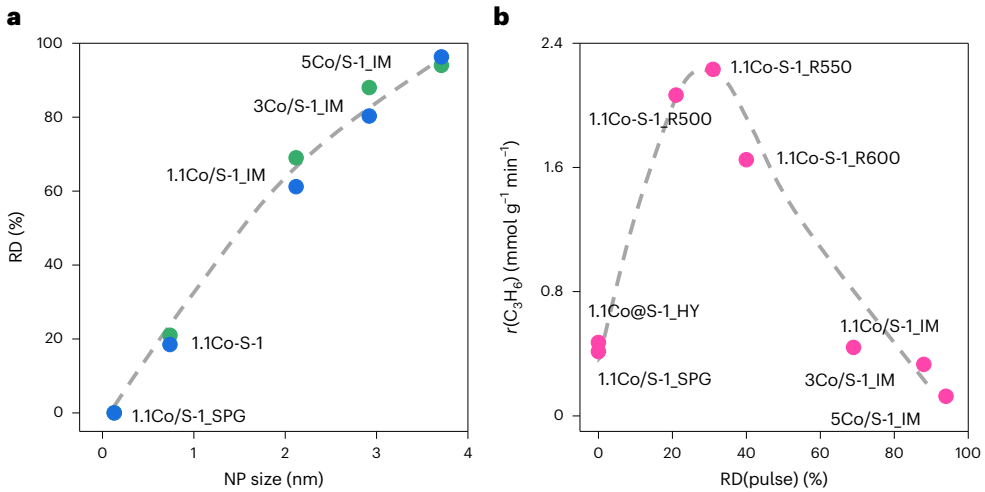

Fig. 5 | CoO_x reducibility and PDH activity of various S-1-based catalysts. **a**, Average reduction degree of silicalite-1-supported CoO_x species (NP) versus their size (green circles, RD(pulse); blue circles, RD(TPR)). The RD(pulse) and RD(TPR) data are provided in Supplementary Table 14. The *x*Co/S-1_IM catalysts were prepared by an impregnation method. **b**, The initial rate of propene formation versus RD(pulse) for a variety of catalysts.

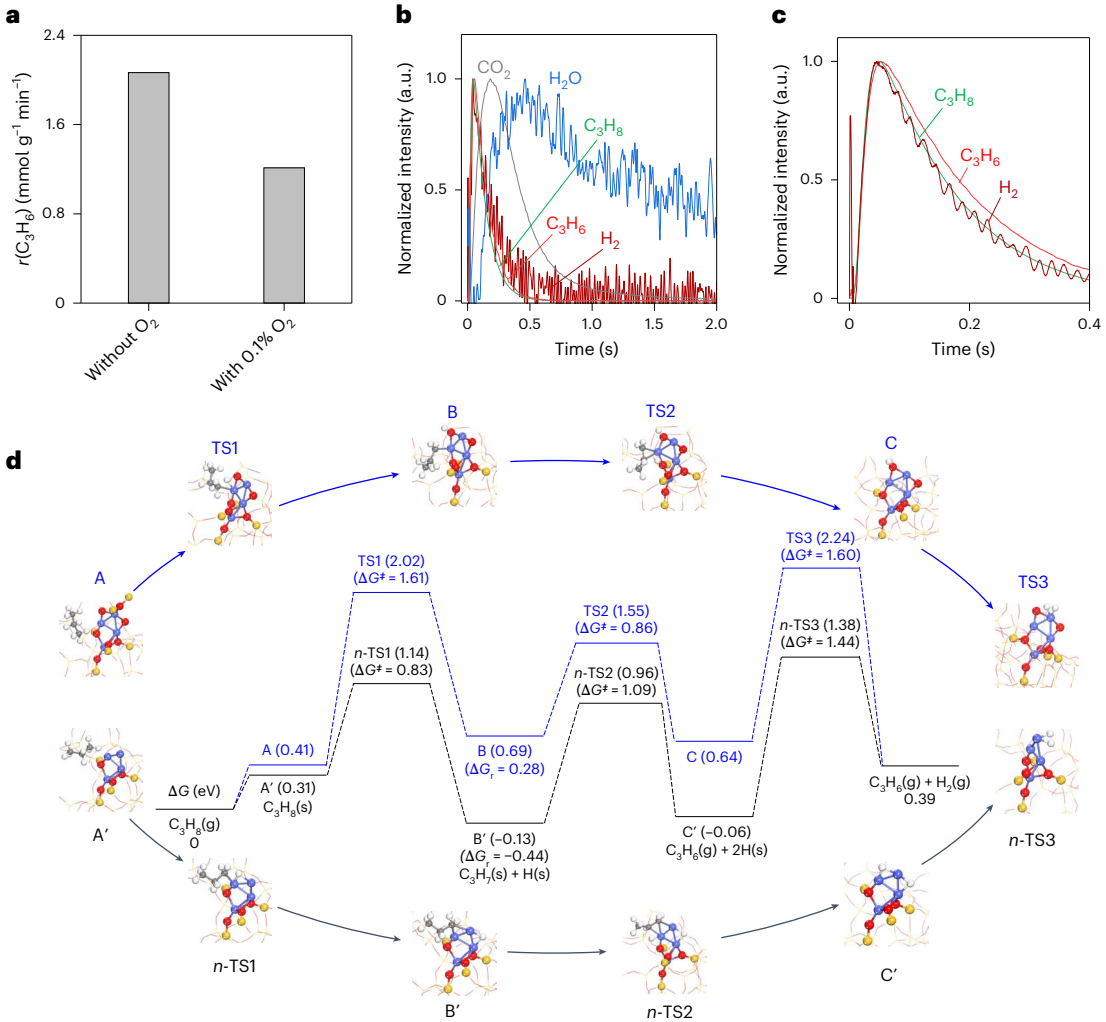

Fig. 6 | Active species and mechanism. **a**, The initial propene formation rate over 1.1Co-S-1 in the absence and presence of co-fed oxygen. Reaction conditions: T = 500 °C, 40 vol% C_3H_8 in N_2 or N_2 containing 0.1 vol% O_2, and WHSV(C_3H_8) = 70.7 h^{-1}. **b**,**c**, Transient responses recorded upon pulsing C_3H_8/Ar = 1:1 over 1.1Co-S-1 after oxidation (**b**) and reduction (**c**) at 500 °C. **d**, Gibbs free-energy profiles of the PDH reaction on $(Si{-}O)_4Co_4O_2$ (blue) and $(Si{-}O)_4Co_4$ (black). Optimization was performed at the PBE-D3 level of theory and Gibbs correction at 773 K. The corresponding energies ($\Delta G^{\ddagger}$ or ΔG_r) of the elementary steps are given in parentheses. In the structures, blue, red, yellow, grey and white balls represent Co, O, Si, C and H atoms, respectively.

responses of C_3H_8, H_2 and C_3H_6 to dimensionless time following Gleaves et al.[34] to account for the strongly different diffusivities of H_2 and C_3H_6/C_3H_8. As expected, the dimensionless time to maximum H_2 concentration is substantially longer than that of C_3H_6 (Supplementary Fig. 47). Based on this analysis, the formation of H_2 should be the rate-limiting step in the PDH reaction.

We performed DFT calculations to identify molecular-level pathways for PDH to propene over oxidized or partially reduced CoO_x clusters. The most stable $(Si–O)_4Co_4O_2$ structure, representing an oxidized CoO_x cluster, was used to calculate both the oxidative dehydrogenation of propane (ODP) and PDH reactions (Fig. 6d, Supplementary Figs. 48–50 and Supplementary Note 1), while the $(Si–O)_4Co_4$ model, representing a partially reduced CoO_x cluster, was used to calculate PDH only (Fig. 6d and Supplementary Figs. 51–54). The calculations predict that ODP involving Co=O in $(Si–O)_4Co_4O_2$ is kinetically more favourable but thermodynamically less favourable than PDH. For TS4 versus TS3 in Supplementary Fig. 50, representing the most favourable ODP and PDH pathways, the apparent Gibbs free-energy barrier ($\Delta G^{\ddagger}$) is 1.56 eV versus 2.24 eV, while the Gibbs free energy of reaction (ΔG_r) is 0.61 eV versus 0.39 eV. Therefore, we can rationally propose that $(Si–O)_4Co_4O_2$ is converted to $(Si–O)_4Co_4$ under the reaction conditions, as proven experimentally in the C_3H_8 pulse experiments (Fig. 6b). The adsorption of propane (A′) on $(Si–O)_4Co_4$ is endergonic by 0.31 eV (Fig. 6d). The dissociation of the first C–H bond (*n*-TS1), leading to the formation of adsorbed *n*-C_3H_7 and H species (B′), has a $\Delta G^{\ddagger}$ of 0.83 eV and is exergonic by 0.44 eV. The cleavage of the C–H bond in *n*-C_3H_7 (*n*-TS2) to form adsorbed propene and another H species (C′) requires a $\Delta G^{\ddagger}$ of 1.09 eV and is endergonic by 0.07 eV. In agreement with the results of the C_3H_8 pulse experiments presented in Supplementary Fig. 47, the recombination of two surface H atoms (*n*-TS3) to yield gaseous H_2 seems to be the rate-limiting step, with a $\Delta G^{\ddagger}$ of 1.44 eV.

Conclusions

The work presented here demonstrates the progress achieved in the development of Co-based catalysts using S-1 as a support with industrially relevant performance in the PDH reaction. This has been made possible by the creation of a specific active site consisting of Co^0 atoms on top of subnanometre CoO_x clusters. Their oxidized precursors are prepared through a pH-controlled reaction of aqueous Co^{2+} complexes with defective OH groups in S-1 and transform into the partially reduced active sites under PDH conditions. Their catalytic performance can be further improved by precisely controlling the number of cobalt atoms in their structure. The results presented here provide a basis for the purposeful development not only of Co-containing catalysts but also of other metal oxide catalysts that can be partially converted to metals under reaction conditions.

Methods

Materials

Tetraethyl orthosilicate (TEOS, Sigma-Aldrich), $Co(NO_3)_2{\cdot}6H_2O$ (99%, Sigma-Aldrich), tetrapropylammonium hydroxide (TPAOH, Sigma-Aldrich), cetyltrimethylammonium bromide (CTAB, Sigma-Aldrich), dodecylamine (DDA, 99%, Aldrich), H_2PtCl_6 solution (8 wt% H_2PtCl_6, Merck), $SnCl_2{\cdot}2H_2O$ (99.99%, Sigma-Aldrich), ethylenediamine (EDA, 99%, Merck), ethanol (99.9%, Thermo Fisher), NH_4OH (25 wt%, Carl Roth), NaOH (99%, Sigma-Aldrich), $(NH_4)_2(SiF_6)$ (98%, Thermo Scientific), SiO_2 (Davisil, grade 646, Sigma-Aldrich) and Al_2O_3 (Saint-Gobain) were used as received.

Catalyst synthesis. S-1 was prepared according to a previous report[7]. TEOS, TPAOH and deionized water (H_2O) were mixed in a mass ratio of 1:0.244:0.518 and stirred at room temperature for 6 h, followed by hydrothermal treatment at 100 °C for 48 h. After cooling to room temperature, the resulting solid was separated by centrifugation, washed with H_2O, dried at 100 °C and finally calcined at 550 °C for 6 h. Na-S-1 was prepared using a similar procedure, except that NaOH was added to the initial sol–gel mixture in a TEOS, TPAOH, H_2O and NaOH mass ratio of 1:0.244:0.518:0.0096.

HMS was synthesized using a mixture of DDA, ethanol, H_2O and TEOS in a mass ratio of 1:8.28:9.72:4.16. After stirring at room temperature for 24 h, the resulting gel was filtered and washed several times with H_2O. HMS was obtained after drying at 100 °C overnight and calcination at 550 °C for 6 h.

MCM-41 was synthesized by first mixing 500 g H_2O, 200 g ethanol and 17 g CTAB at room temperature. Then, 42 g TEOS was added to the solution, followed by 0.4 ml concentrated HCl to obtain an acidic solution (pH 2). The solution became clear after a short time. After 30 min, the pH was adjusted to 8–9 by adding NH_4OH. The white solid product obtained by filtration was washed with H_2O, dried at room temperature for 24 h and then calcined at 550 °C for 5 h.

To prepare the S-1_L support, 21.9 g TPAOH was added to 118 g H_2O and the mixture stirred for 15 min. Then, 36 g silica sol was added to the above solution and stirred for 6 h, followed by hydrothermal treatment at 170 °C for 48 h. After cooling to room temperature, the resulting solid was separated by centrifugation, washed with H_2O and dried at 100 °C. Finally, the obtained precursor was calcined at 550 °C for 6 h.

To synthesize the S-1_F support, 4 g S-1 was dispersed in 216 g H_2O and agitated at 80 °C for 1 h to obtain solution A. Then, 0.2 g $(NH_4)_2[SiF_6]$ was added to 100 g H_2O and the mixture stirred for 10 min to obtain solution B, which was added dropwise to solution A. The resulting solution was stirred at 80 °C for 71 h. The obtained solid was recovered by centrifugation and washed with H_2O six times, followed by drying at 100 °C overnight and calcination at 550 °C in air for 4 h.

To prepare supports with different densities of silanol defects, 5 g β-zeolites with different Si/Al ratios (25 and 150) were treated with 100 ml concentrated HNO_3 at 120 °C for 10 h. The resulting solids were washed with H_2O three times and dried at 100 °C for 10 h. The dried samples were dispersed in 100 ml of 2 M HNO_3 and stirred at room temperature for 12 h. Afterwards, the treated zeolites were washed with H_2O until the pH reached 7, followed by drying at 100 °C for 10 h to obtain the final samples, abbreviated as Deal Beta-25 and Deal Beta-150, respectively.

A typical procedure for the preparation of catalysts by the SEA method is described here for the 1.1Co-S-1 catalyst. First, 0.5 g S-1 was suspended in 7 ml H_2O adjusted to pH 11 with NH_4OH. Then, 0.0249 g $Co(NO_3)_2{\cdot}6H_2O$ was dissolved in 0.75 ml NH_4OH, followed by the addition of 0.75 ml H_2O. The cobalt precursor solution was slowly added to the S-1 suspension under stirring for 30 min. The resulting suspension was filtered and washed with H_2O five times. The obtained sample was dried at 100 °C overnight, followed by calcination at 550 °C in air for 2 h to obtain the final catalyst. Catalysts with different Co loadings are denoted as *x*Co-S-1, where *x* is the mass concentration of cobalt determined by inductively coupled plasma. Catalysts based on the other supports are abbreviated as *x*Co-SiO_2, *x*Co-MCM-41, *x*Co-HMS, *x*Co-S-1_L, *x*Co-S-1_F, *x*Co-Deal Beta-25, *x*Co-Deal Beta-150 and *x*Co-Na-S-1.

*x*Co/S-1_IM catalysts were prepared by an incipient wetness impregnation method using an aqueous solution of $Co(NO_3)_2{\cdot}6H_2O$, followed by drying at 100 °C for 12 h and calcination in flowing air at 550 °C for 6 h.

The 1.1Co@S-1_HY catalyst was synthesized by a hydrothermal method using TEOS and $Co(NO_3)_2{\cdot}6H_2O$ as the silicon and cobalt sources, respectively, TPAOH as the structure-directing agent and EDA as a stabilizer to form a complex with Co^{2+}. The starting gel with a SiO_2/Co/EDA/TPAOH/H_2O molar composition of 1.0:0.011:0.83:0.40:35 was crystallized in a Teflon-lined autoclave at 170 °C for 96 h and then filtered, dried and calcined at 550 °C.

The 1.1Co/S-1_SPG catalyst was synthesized by solid-phase grinding. First, 0.055 g $Co(NO_3)_2{\cdot}6H_2O$ was dissolved in 1 ml H_2O. The resulting solution was mixed with 1.0 g S-1 and manually ground in a mortar using a pestle for 60 min. After drying at 100 °C overnight, the sample

was pretreated with 5 vol% H_2/Ar (10 ml min^{-1}) at room temperature for 30 min and heated (1 °C min^{-1}) to 550 °C followed by tempering at this temperature for 6 h.

An analogue of commercial K-CrO_x/Al_2O_3 was synthesized according to a previous method[35]. Briefly, the desired amounts of CrO_3 and KOH were separately dissolved in water. These solutions were then mixed, followed by the addition of Al_2O_3. The catalyst was collected after drying and calcined at 760 °C for 4 h. The amounts of Cr_2O_3 and K_2O obtained were 19.7 and 0.93 wt%, respectively.

An analogue of industrial PtSn/Al_2O_3 (0.5 wt% Pt and 1.5 wt% Sn) was prepared according to a previous report[36]. First, 0.628 g H_2PtCl_6 and 0.145 g $SnCl_2{\cdot}2H_2O$ were dissolved in 30 ml of 99.9% ethanol. Then, 5 g Al_2O_3 was impregnated with this solution. The resulting sample was dried at 100 °C for 12 h and then calcined in air at 560 °C for 3 h.

Catalyst characterization. XRD patterns of the prepared catalysts were recorded on a Bruker D8 Advance diffractometer at 40 kV and 100 mA using Cu Kα radiation (0.15406 nm).

Ex situ UV–visible spectra were recorded between 200 and 900 nm on a Shimadzu UV-2600 spectrophotometer using $BaSO_4$ as a white standard.

High-resolution TEM images were recorded on an FEI Talos 200X microscope with a working voltage of 200 kV. AC-HAADF-STEM experiments were performed on an FEI Titan Cubed Themis G2 300 device at 300 kV.

TPR experiments with H_2 were carried out in a set-up developed in house consisting of eight individually heated continuous-flow fixed-bed quartz reactors. First, 100 mg of each sample was initially calcined in air at 500 °C for 1 h, cooled to room temperature in the same flow and then treated with Ar for 15 min. The catalysts were then heated (10 °C min^{-1}) to 900 °C in a flow of 5 vol% H_2/Ar (10 ml min^{-1}). An on-line mass spectrometer (Pfeiffer Vacuum OmniStar GSD 320) was used to record the signals at m/z = 2 (H_2) and 40 (Ar), with the latter serving as a standard.

Solid-state ^{1}H magic-angle-spinning (MAS) NMR spectra were recorded using a Bruker Avance III 500 spectrometer at a resonance frequency of 500 MHz using a single pulse sequence with a recycle delay of 100 s, a scan number of 16, a π/2 pulse width of 3.05 µs and a spin rate of 20 kHz. A standard 3.2-mm double-bearing Bruker MAS probe was used. The samples were first dehydrated at 673 K for 10 h and then placed in 3.2-mm MAS rotors in a glove box under Ar. The ^{1}H MAS NMR measurements were quantified by comparing the intensities of the signals with that of adamantane as external standard. Decomposition and simulation of the NMR spectra were performed using the Dmfit software.

In situ diffuse reflectance FTIR spectra were recorded in the range of 600–4,000 cm^{-1} at a resolution of 4 cm^{-1} using a Bruker VERTEX 70 spectrometer with a ZnSe window. Each sample was first heated (10 K min^{-1}) to 500 °C in N_2 (10 ml min^{-1}), then calcined in air (10 ml min^{-1}) at 500 °C for 30 min and flushed with N_2 (10 ml min^{-1}) for 15 min.

In situ UV–visible measurements were performed using an Avantes spectrometer (AvaSpes-2048-USB2-RM) equipped with a high-temperature reflectance UV–visible probe, an Ava-Light-DH-S-BAL light source and a charge-coupled device detector. The probe, consisting of six radiating optical fibres and one reading fibre, was threaded through the furnace to face the wall of the quartz reactor at the position of the catalyst (100 mg). Each sample was first heated (10 °C min^{-1}) to 500 °C in N_2 (10 ml min^{-1}), calcined in air (10 ml min^{-1}) at 500 °C for 30 min and then flushed with N_2 (10 ml min^{-1}) for 15 min. A feed containing 40 vol% H_2 in N_2 (10 ml min^{-1}) was supplied to the samples and UV–visible spectra were recorded between 200 and 800 nm. $BaSO_4$ (99.998%, Aldrich) was used as a white standard.

Pseudo in situ XPS measurements were performed in a laboratory near-ambient-pressure XPS system (SPECS Surface Nano Analysis). The set-up included a differentially pumped Phoibos 150 electron energy analyser and a monochromated Al Kα radiation source (E = 1,486.6 eV) operated at 70 W and 15 kV. The system was connected to a high-pressure cell (HPC 20, SPECS Surface Nano Analysis), which offered sample heating by a halogen lamp and was equipped with four mass flow controllers at the inlet and a manual back-pressure regulator (Swagelok) at the outlet. Samples were heated to 500 °C (10 °C min^{-1}) in N_2 (10 ml min^{-1}), then fed with 20 vol% O_2 in N_2 (10 ml min^{-1}) for 30 min, cooled in N_2 (heater off) and transferred to the measurement chamber. Each sample was pressed on a stainless-steel sample plate using a laboratory press with a diameter of 5 mm and a load of about 1 t. The temperature was monitored by a thermocouple on the sample plate pressed on the sample surface. Electron binding energies were obtained with charge compensation using a flood electron source and referenced to the Si $2p_{3/2}$ peak of SiO_2 at 103.3 eV. The peaks were deconvoluted by means of Gaussian–Lorentzian curves using the Unifit 2023 software. Peak areas were normalized by the transmission function of the spectrometer and the element-specific Scofield sensitivity factor.

XAS spectra at the Co K absorption edge were recorded in transmission mode at the P65 beamline of the PETRA III synchrotron radiation source (DESY). Higher harmonics were rejected by a pair of Si plane mirrors installed in front of the monochromator. The X-ray photon energy was selected using a Si(111) double-crystal monochromator and the beam size was adjusted by means of slits to 0.4 mm (vertical) × 2.0 mm (horizontal). The spectra were normalized and the background of the EXAFS spectra was subtracted using the ATHENA program of the IFEFFIT software package[37]. The k^2-weighted EXAFS functions were Fourier-transformed in the k range of 3.0–11.5 $Å^{-1}$ and multiplied by a Hanning window with a sill size of 1 $Å^{-1}$. The FT-EXAFS spectra were not corrected for the phase shift. For the in situ measurements, the 1.1Co-S-1 catalyst with a sieve fraction of 100–200 µm was loaded in an in situ microreactor (quartz capillary, 1.5-mm diameter and 0.02-mm wall thickness). The sample was heated (10 °C min^{-1}) to 500 °C in He (20 ml min^{-1}) and fed with a flow of 50 vol% H_2 in He for 30 min, followed by a flow of 50 vol% C_3H_8 in He for 30 min. The sample was kept at room temperature for 10 min before recording the spectra.

Transient experiments with submillisecond resolution were performed in the TAP-2 reactor system[34]. Each catalyst (35 mg, 315–715 µm fraction) was placed in a quartz tube reactor and fixed within its isothermal zone between two layers of quartz particles (250–355 µm). The catalysts were initially treated either oxidatively or reductively. A fresh sample was used for each treatment. During oxidative treatment, the catalysts were heated to 500 °C in N_2 (10 ml min^{-1}) and fed (8 ml min^{-1}) with 50 vol% O_2 in N_2 for 30 min. During reductive treatment, the catalysts were initially oxidized as described above, treated with N_2 (8 ml min^{-1}) for 15 min and then exposed to a flow (10 ml min^{-1}) of 20 vol% H_2 in N_2 for 30 min. After evacuation to ~10^{-5} Pa, C_3H_8/Ar = 1:1 was pulsed ((3–6) × 10^{15} molecules per pulse) at 500 °C. The mixture was prepared using C_3H_8 (Linde, 3.5) and Ar (Air Liquide, 5.0) without additional purification.

The composition of the gas mixture at the reactor outlet was determined by quadrupole mass spectrometry (HAL RC 301 Hiden Analytical) using the following m/z values: 44 (CO_2 and C_3H_8), 42 (C_3H_8 and C_3H_6), 41 (C_3H_8 and C_3H_6), 29 (C_3H_8), 28 (C_3H_8, C_2H_8, CO_2 and CO), 18 (H_2O), 2 (H_2) and 40 (Ar). The pulses for each m/z were repeated ten times and averaged to improve the signal-to-noise ratio. The contribution of different compounds to the respective m/z was estimated using standard fragmentation patterns, determined in separate experiments.

Computation details. Spin-polarized periodic DFT calculations were performed using the Vienna ab initio simulation package[38,39]. The electron exchange and correlation energies were treated with the generalized gradient approximation in the Perdew–Burke–Ernzerhof (GGA-PBE) functional[40]. The cut-off energy was set to 400 eV. Geometry optimization was performed using the PBE functional with van der

Waals dispersion correction (GGA-PBE-D3)[41] and converged until the forces acting on the atoms were less than 0.02 eV $Å^{-1}$ and the energy difference was less than 10^{-4} eV. The climbing image nudged elastic band method was applied to identify transition states[42]. Gibbs free-energy correction was made using the VASPKIT program[43].

Calculations were performed using the MFI zeolite with a hydroxy nest at the T5 site. This site is located at the intersection of the straight and sinusoidal channels and has a larger environmental volume or space to accommodate molecules for reactions.

Based on our experimental XANES data, the fresh catalyst contains $Co^{II}O_x$ species. As clusters containing a Co_4 unit were used as representative models for dehydrogenation reactions[10,33], we constructed an embedded Co_4O_6 cluster with Co^{II} at the hydroxy nest of the T5 site by consuming all OH groups ($4OH + 2Co(OH)_2 \rightarrow Co_2O_4 + 4H_2O$) and adding a Co_2O_2 unit ($Co_2O_4 + 2CoO$). Structure optimization resulted in two options: a nearly planar cluster (0 eV) and a less stable cubic-like cluster (1.47 eV; Supplementary Fig. 43). The former cluster was used to create a cluster with reduced cobalt by removing two oxygen atoms, resulting in a Co_4O_4 unit ($Co_2O_4 + 2Co$) that has two formal Co^{II} and two formal Co^0 centres. Therefore, we used the oxidized planar Co_4O_6 ($(Si–O)_4Co_4O_2$) and reduced Co_4O_4 ($(Si–O)_4Co_4$) clusters (Supplementary Fig. 44) for our calculations.

Catalytic tests. Catalytic tests were performed under continuous-flow conditions at 1 bar. The rate of propene formation ($r(C_3H_6)$) was determined at a propane conversion below 10% to ensure differential reactor operation. The catalysts (20 mg, 315–710 µm) were heated (10 °C min^{-1}) to 500 °C in N_2 (10 ml min^{-1}), followed by feeding with air for 30 min and purging with N_2 for 15 min. They were then reduced in a flow of 50 vol% H_2 in N_2 (10 ml min^{-1}) for 30 min at 500 °C. The treated catalysts were tested at 500 °C (40 vol% C_3H_8 in N_2 containing 0–0.1 vol% O_2, 30 ml min^{-1}).

We also performed two tests consisting of 120 PDH/regeneration cycles at 500 and 525 °C using 20 vol% C_3H_8 in N_2 at a WHSV of 4.7 h^{-1}, and 20 PDH/regeneration cycles with 40 vol% C_3H_8 in N_2 at 500 and 550 °C with a WHSV of 4.7 and 9.4 h^{-1}, respectively. One full PDH/regeneration cycle lasted for 60 min: PDH lasted for 30 min, followed by flushing with N_2 (10 ml min^{-1}) for 10 min, calcination with air (10 ml min^{-1}) for 10 min and flushing again with N_2 (10 ml min^{-1}) for 10 min.

In a long-term test, 1.1Co-S-1, $PtSn/Al_2O_3$ and K-CrO_x/Al_2O_3 (20 mg, 315–710 µm) were first heated (10 °C min^{-1}) to 500 °C in N_2, followed by feeding with air for 30 min and purging with N_2 for 15 min. Then, the catalysts were reduced in a flow of 50 vol% H_2 in N_2 (10 ml min^{-1}) for 30 min at 500 °C and then tested at 500 °C (40 vol% C_3H_8 in N_2, 10 ml min^{-1}). In view of the industrial relevance, we also performed tests using 100 mg catalyst with a feed of 95 vol% C_3H_8 in N_2 (18.9 ml min^{-1}) at 500, 550 and 600 °C. An additional test was conducted at 500 °C for 96 h using the same feed (5 ml min^{-1}), but with 50 mg of catalyst. The reactants and reaction products were analysed following the procedures outlined in the Supplementary Methods.

Data availability

The data supporting the findings of this study are available in the Article and its Supplementary Information or from the authors upon reasonable request. Source data are provided with this paper.

References

1. Chen, S. et al. Propane dehydrogenation: catalyst development, new chemistry, and emerging technologies. *Chem. Soc. Rev.* **50**, 3315–3354 (2021).
2. Bai, P. et al. Fluid catalytic cracking technology: current status and recent discoveries on catalyst contamination. *Catal. Rev.* **61**, 333–405 (2019).
3. Akah, A., Williams, J. & Ghrami, M. An overview of light olefins production via steam enhanced catalytic cracking. *Catal. Surv. Asia* **23**, 265–276 (2019).
4. Rabenhorst, R. On purpose—what's driving new propane dehydrogenation projects in North America? *Daily Energy Posts* https://rbnenergy.com/daily-posts/blog/whats-driving-new-propane-dehydrogenation-projects-north-america (2019).
5. Otroshchenko, T., Jiang, G. Y., Kondratenko, V. A., Rodemerck, U. & Kondratenko, E. V. Current status and perspectives in oxidative, non-oxidative and CO_2-mediated dehydrogenation of propane and isobutane over metal oxide catalysts. *Chem. Soc. Rev.* **50**, 473–527 (2021).
6. Zhao, D. et al. Controlling reaction-induced loss of active sites in ZnO_x/silicalite-1 for durable nonoxidative propane dehydrogenation. *ACS Catal.* **12**, 4608–4617 (2022).
7. Zhao, D. et al. In situ formation of ZnO_x species for efficient propane dehydrogenation. *Nature* **599**, 234–238 (2021).
8. Xie, L. et al. Propane dehydrogenation catalyzed by in-situ partially reduced zinc cations confined in zeolites. *J. Energy Chem.* **63**, 262–269 (2021).
9. Wang, W. et al. Single Co sites in ordered SiO_2 channels for boosting nonoxidative propane dehydrogenation. *ACS Catal.* **12**, 2632–2638 (2022).
10. Song, S. et al. In situ encapsulated subnanometric CoO clusters within silicalite-1 zeolite for efficient propane dehydrogenation. *AlChE J.* **68**, e17451 (2022).
11. Hu, Z. P. et al. Atomic insight into the local structure and microenvironment of isolated Co-motifs in MFI zeolite frameworks for propane dehydrogenation. *J. Am. Chem. Soc.* **144**, 12127–12137 (2022).
12. Hu, B. et al. Isolated Fe^{II} on silica as a selective propane dehydrogenation catalyst. *ACS Catal.* **5**, 3494–3503 (2015).
13. Xu, G. et al. Ferric single-site catalyst confined in a zeolite framework for propane dehydrogenation. *Angew. Chem. Int. Ed.* **62**, e202305915 (2023).
14. Ni, L. et al. Highly active and selective sites for propane dehydrogenation in zeolite Ga-BEA. *J. Am. Chem. Soc.* **144**, 12347–12356 (2022).
15. Li, Y. et al. The nature of VO_x structures in HMS supported vanadium catalysts for non-oxidative propane dehydrogenation. *J. Catal.* **413**, 658–667 (2022).
16. Rodemerck, U., Stoyanova, M., Kondratenko, E. V. & Linke, D. Influence of the kind of VO_x structures in VO_x/MCM-41 on activity, selectivity and stability in dehydrogenation of propane and isobutane. *J. Catal.* **352**, 256–263 (2017).
17. Zhang, Y. et al. Control of coordinatively unsaturated Zr sites in ZrO_2 for efficient C–H bond activation. *Nat. Commun.* **9**, 3794 (2018).
18. Otroshchenko, T. et al. ZrO_2-based alternatives to conventional propane dehydrogenation catalysts: active sites, design, and performance. *Angew. Chem. Int. Ed.* **54**, 15880–15883 (2015).
19. Chen, C., Zhang, S., Wang, Z. & Yuan, Z.-Y. Ultrasmall Co confined in the silanols of dealuminated beta zeolite: a highly active and selective catalyst for direct dehydrogenation of propane to propylene. *J. Catal.* **383**, 77–87 (2020).
20. Li, Y. et al. Active species and fundamentals of their creation in Co-containing catalysts for efficient propane dehydrogenation to propylene. *Chem. Eng. J.* **460**, 141778 (2023).
21. Liu, Q. et al. Stable cobalt–zeolite propane-dehydrogenation catalysts enabled by reaction-driven reconstruction. *Angew. Chem. Int. Ed.* **64**, e202505628 (2025).
22. Wu, L. et al. Atomically dispersed Co^{2+} sites incorporated into a silicalite-1 zeolite framework as a high-performance and coking-resistant catalyst for propane nonoxidative dehydrogenation to propylene. *ACS Appl. Mater. Interfaces* **13**, 48934–48948 (2021).

23. Dai, Y. et al. γ-Al_2O_3 sheet-stabilized isolate Co^{2+} for catalytic propane dehydrogenation. *J. Catal.* **381**, 482–492 (2020).
24. Hu, B. et al. Selective propane dehydrogenation with single-site Co^{II} on SiO_2 by a non-redox mechanism. *J. Catal.* **322**, 24–37 (2015).
25. Estes, D. P. et al. C–H activation on Co,O sites: isolated surface sites versus molecular analogs. *J. Am. Chem. Soc.* **138**, 14987–14997 (2016).
26. Liu, L. et al. Rivet of cobalt in siliceous zeolite for catalytic ethane dehydrogenation. *Chem* **9**, 637–649 (2023).
27. Li, X., Wang, P., Wang, H. & Li, C. Effects of the state of Co species in Co/Al_2O_3 catalysts on the catalytic performance of propane dehydrogenation. *Appl. Surf. Sci.* **441**, 688–693 (2018).
28. Zhang, Q. et al. Understanding the reaction-induced restructuring of CoO_x species in silicalite-1 to control selectivity in non-oxidative dehydrogenation of propane. *Chin. J. Catal.* **74**, 108–119 (2025).
29. Motagamwala, A. H., Almallahi, R., Wortman, J., Igenegbai, V. O. & Linic, S. Stable and selective catalysts for propane dehydrogenation operating at thermodynamic limit. *Science* **373**, 217–222 (2021).
30. Boroń, P. et al. Effect of Co content on the catalytic activity of CoSiBEA zeolites in N_2O decomposition and SCR of NO with ammonia. *Catal. Today* **258**, 507–517 (2015).
31. Das, T., Tosoni, S. & Pacchioni, G. Role of support in tuning the properties of single atom catalysts: Cu, Ag, Au, Ni, Pd, and Pt adsorption on SiO_2/Ru, SiO_2/Pt, and SiO_2/Si ultrathin films. *J. Chem. Phys.* **154**, 134706 (2021).
32. Schlexer, P. & Pacchioni, G. Adsorption and dimerization of late transition metal atoms on the regular and defective quartz (001) surface. *Top. Catal.* **60**, 459–470 (2017).
33. Lee, S. et al. Subnanometer cobalt oxide clusters as selective low temperature oxidative dehydrogenation catalysts. *Nat. Commun.* **10**, 954 (2019).
34. Gleaves, J. T., Yablonskii, G. S., Phanawadee, P. & Schuurman, Y. TAP-2: an interrogative kinetics approach. *Appl. Catal. A* **160**, 55–88 (1997).
35. Fridman, V. Catalyst for dehydrogenation of hydrocarbons. US patent 8,101,541 B2 (2012).
36. Iglesias-Juez, A. et al. A combined in situ time-resolved UV–Vis, Raman and high-energy resolution X-ray absorption spectroscopy study on the deactivation behavior of Pt and PtSn propane dehydrogenation catalysts under industrial reaction conditions. *J. Catal.* **276**, 268–279 (2010).
37. Ravel, B. & Newville, M. ATHENA, ARTEMIS, HEPHAESTUS: data analysis for X-ray absorption spectroscopy using IFEFFIT. *J. Synchrotron Radiat.* **12**, 537–541 (2005).
38. Kresse, G. & Furthmüller, J. Efficient iterative schemes for ab initio total-energy calculations using a plane-wave basis set. *Phys. Rev. B* **54**, 11169 (1996).
39. Kresse, G. & Furthmüller, J. Efficiency of ab-initio total energy calculations for metals and semiconductors using a plane-wave basis set. *Comput. Mater. Sci.* **6**, 15–50 (1996).
40. Perdew, J. P., Burke, K. & Ernzerhof, M. Generalized gradient approximation made simple. *Phys. Rev. Lett.* **77**, 3865–3868 (1996).
41. Grimme, S., Antony, J., Ehrlich, S. & Krieg, H. A consistent and accurate ab initio parametrization of density functional dispersion correction (DFT-D) for the 94 elements H-Pu. *J. Chem. Phys.* **132**, 154104 (2010).
42. Henkelman, G., Uberuaga, B. P. & Jónsson, H. A climbing image nudged elastic band method for finding saddle points and minimum energy paths. *J. Chem. Phys.* **113**, 9901–9904 (2000).
43. Wang, V., Xu, N., Liu, J.-C., Tang, G. & Geng, W.-T. VASPKIT: a user-friendly interface facilitating high-throughput computing and analysis using VASP code. *Comput. Phys. Commun.* **267**, 108033 (2021).

Acknowledgements

Financial support from the State of Mecklenburg-Vorpommern is gratefully acknowledged. This work was supported by the National Natural Science Foundation of China (grant nos. 22225807, 21961132026 and 22021004), the National Key Research and Development Program (nos. 2020YFA0210903 and 2021YFA1501304), the Fundamental Research Program of Shanxi Province (202403021211195) and Shanxi Scholarship Council of China (2024-005). We acknowledge DESY (Hamburg, Germany), a member of the Helmholtz Association HGF, for the provision of experimental facilities. Parts of this research were carried out at PETRA III, DESY, and we thank E. Welter for assistance in using beamline P65. Beamtime was allocated for proposals I-20230372 and I-20240852.

Author contributions

E.V.K. initiated and led the whole project. E.V.K. and G.J. supervised and coordinated the project. Q.Z. prepared all of the catalysts and carried out the characterization measurements and catalytic tests. Q.Z. and E.V.K. wrote the first draft of the paper. X.T. and H.J. performed DFT calculations and wrote the corresponding part of the paper. Y.L. prepared some of the catalysts. E.A.F., D.E.D. and D.Z. performed the XAS experiments and analysed the results. V.A.K. carried out the TAP tests and analysed the results. X.D. tested some of the catalysts. T.Y. and C.D. performed the techno-economic assessment and analysed the results. H.C. and S.X. performed the NMR characterization and analysed the results. A.Z. performed the in situ UV–visible characterization and analysed the results. S.B. performed the in situ XPS characterization and analysed the results. Y.W., Z.Z. and C.X. participated in the discussion. All authors contributed to the discussion of the research and approved the final version of the paper.

Funding

Open access funding provided by Leibniz-Institut für Katalyse e.V. (LIKAT Rostock).

Competing interests

The authors declare no competing interests.

Additional information

Supplementary information The online version contains supplementary material available at https://doi.org/10.1038/s41929-026-01488-w.

Correspondence and requests for materials should be addressed to Guiyuan Jiang, Haijun Jiao or Evgenii V. Kondratenko.

Peer review information *Nature Catalysis* thanks the anonymous reviewers for their contribution to the peer review of this work.